Influence of different rotational speeds on the structural and optical properties of $CsPbBr_3$ perovskite films

YAXIN CHEN[1], FEI ZHAO[2,*], PEIZHI YANG[3]

[1]*School of Electrical and Electronic Engineering, Anhui Institute of Information Technology, Wuhu 241000, China*

[2]*School of Photoelectric Engineering, Changzhou Institute of Technology, Changzhou 213032, China*

[3]*College of Energy and Environmental Science, Yunnan Normal University, Kunming 650500, China*

The all-inorganic $CsPbBr_3$ perovskite film has attracted widespread attention from the academic community due to its excellent air and thermal stability. However, the grain growth of $CsPbBr_3$ perovskite film is uneven. Here, high-quality $CsPbBr_3$ perovskite film was successfully prepared by adjusting the rotational speed. When the rotational speed increases from 1000rpm to 2000rpm, $CsPbBr_3$ perovskite film exhibits higher crystallinity, better uniformity, larger average grain size (583nm), and smaller optical band gap (2.341eV). As the rotational speed further increases to 3000rpm, the crystallinity and uniformity of $CsPbBr_3$ perovskite film deteriorate and its average grain size decreases and its optical band gap increases. Therefore, the optimal rotational speed is 2000rpm under the condition of this experiment.

(Received April 23, 2025; accepted December 4, 2025)

Keywords: $CsPbBr_3$, Crystallinity, Uniformity, Optical band gap

1. Introduction

In recent years, all-inorganic cesium-based perovskites have garnered significant attention from researchers due to their high absorption coefficients, tunable optical band gaps, and excellent thermal stability [1-3]. Among these all-inorganic cesium-based perovskites, the most prominent members include $CsPbI_3$, $CsPbI_2Br$, $CsPbBr_2I$, and $CsPbBr_3$[4-7]. These materials are primarily applied in the field of solar cells. Among the aforementioned perovskites, $CsPbI_3$ exhibits the smallest optical band gap (1.73eV), which maximizes the utilization of the solar spectrum. However, $CsPbI_3$ suffers from a relatively low tolerance factor, leading to poor thermal stability [8-10]. The phase transitions in $CsPbI_3$ can be readily observed at room temperature. In comparison, $CsPbI_2Br$ demonstrates an improved tolerance factor and mitigates phase instability issues [11]. Additionally, $CsPbI_2Br$ possesses a relatively low optical bandgap (1.9eV) while maintaining good thermal stability. Nevertheless, $CsPbI_2Br$ exhibits poor stability under high humidity conditions, which remains a significant barrier to practical applications [12]. $CsPbBr_2I$ shows significantly enhanced stability under high humidity environments compared to $CsPbI_2Br$ [13].

Among all-inorganic cesium-based perovskites, $CsPbBr_3$ stands out for its superior thermal and air stability, making it particularly suitable for applications in solar cells [14-18]. Currently, the primary method for fabricating $CsPbBr_3$ perovskite film is the solution spin-coating technique. The preparation process of this method is simple and the cost is low. In previous work, we deposited $CsPbBr_3$ perovskite films by adjusting the number of CsBr spin-coating layers [19]. However, the uniformity of the deposited $CsPbBr_3$ film requires further improvement. To date, there are relatively few reports on the effects of different spin-coating speeds on the structural and optical properties of $CsPbBr_3$ perovskite films. In this study, we deposited $CsPbBr_3$ perovskite films by varying the spin-coating speeds and investigated the influence of different speeds on the crystallinity, uniformity, average grain size, and optical band gap of the films. The results indicate that among the samples prepared at different spin-coating speeds (1000rpm, 2000rpm, and 3000rpm), the sample prepared at 2000rpm exhibits the best overall performance.

2. Experimental methods

2.1. Film preparation

The $CsPbBr_3$ perovskite films were fabricated using a solution spin-coating method. The detailed experimental procedures are as follows. Firstly, 367mg $PbBr_2$ powder was dissolved in 1 ml dimethylformamide (DMF) solution. Subsequently, the precursor solution was spin-coated onto the FTO substrate to obtain $PbBr_2$ films. The spin-coating speeds were adjusted to 1000rpm, 2000rpm and 3000rpm, respectively. The spin-coating duration was adjusted to 30s. Subsequently, the obtained $PbBr_2$ films were heated at 90℃for 30min. Thereafter, 1 ml anhydrous methanol with 14.9mg CsBr powder was spin-coated onto the $PbBr_2$ layer. The rotational speed and time for this step were set to 2000rpm and 30s, respectively. Then, the films were annealed at 250℃ for 5min. This process was repeated for several times. Finally, the high-quality $CsPbBr_3$ film was obtained. It is noteworthy that the entire fabrication process of $CsPbBr_3$ perovskite film was conducted under ambient atmospheric conditions.

2.2. Characterizations

The crystal structure and composition of the $CsPbBr_3$ films were examined with an X-ray diffraction (XRD). The surface morphologies of the $CsPbBr_3$ films were characterized via scanning electron microscopy (SEM). The X-ray photoelectron spectroscopy (XPS) was measured. In addition, the absorption rate of the $CsPbBr_3$ sample was obtained by a UV spectrophotometer.

3. Results and discussions

3.1. Structural analysis

Fig. 1a shows XRD spectra of $CsPbBr_3$ films based on different rotational speeds. From Fig. 1a, it can be observed that two distinct diffraction peaks are present at 21.76° and 30.81 °C, corresponding to the (110) and (200) crystallographic planes, respectively [19]. Interestingly, the diffraction peak intensities of the (110) and (200) planes are not consistent, which is attributed to the preferential orientation growth within the $CsPbBr_3$ film. Additionally, a diffraction peak is observed at 26.56 °C, which corresponds to the crystallographic plane of the FTO substrate [19]. In addition, it can be observed that the peak positions of (110) and (200) crystallographic planes of the samples prepared at different rotational speeds change, which is due to the influence of the surrounding environment during the XRD test. Fig. 1b shows peak intensity images of (110) for $CsPbBr_3$ films based on different rotational speeds. The sample processed at 2000 rpm exhibits the highest intensity of the (110) peak compared with those processed at 1000 rpm and 3000 rpm. Fig. 1c shows peak intensity images of (200) for $CsPbBr_3$ films based on different rotational speeds. When the rotational speed increases from 1000rpm to 2000rpm, the peak intensity of the (200) crystallographic plane is enhanced. However, as the rotational speed further increases to 3000rpm, the peak intensity of the (200) crystallographic plane begins to weaken. The enhancement in the diffraction peak intensity of the (110) crystallographic plane and (200) crystallographic plane indicates improved crystallinity, while the weakening of the peak intensity suggests a deterioration in crystallinity. Therefore, the $CsPbBr_3$ film exhibits optimal crystallinity at a rotational speed of 2000rpm. Fig. 1d shows peak intensity images of FTO crystallographic plane for $CsPbBr_3$ films based on various rotational speeds. As shown in Fig. 1d, when the rotational speed increases from 1000rpm to 2000rpm, the peak intensity of FTO crystallographic plane increases. However, when the rotational speed further increases to 3000rpm, the peak intensity of FTO crystallographic plane decreases. It is well-known that samples prepared on identical FTO substrates should exhibit consistent FTO crystallographic plane intensities by XRD test. Interestingly, the aforementioned experimental results reveal inconsistencies in the FTO crystallographic plane intensities. This phenomenon can be attributed to the presence of a $CsPbBr_3$ crystallographic plane at 26.56 °C. For samples processed at different rotational speeds, the intensity of the $CsPbBr_3$ crystallographic plane at 26.56 °C varies. Consequently, the diffraction peak intensities observed at 26.56 °C in Fig. 1d exhibit discrepancies.

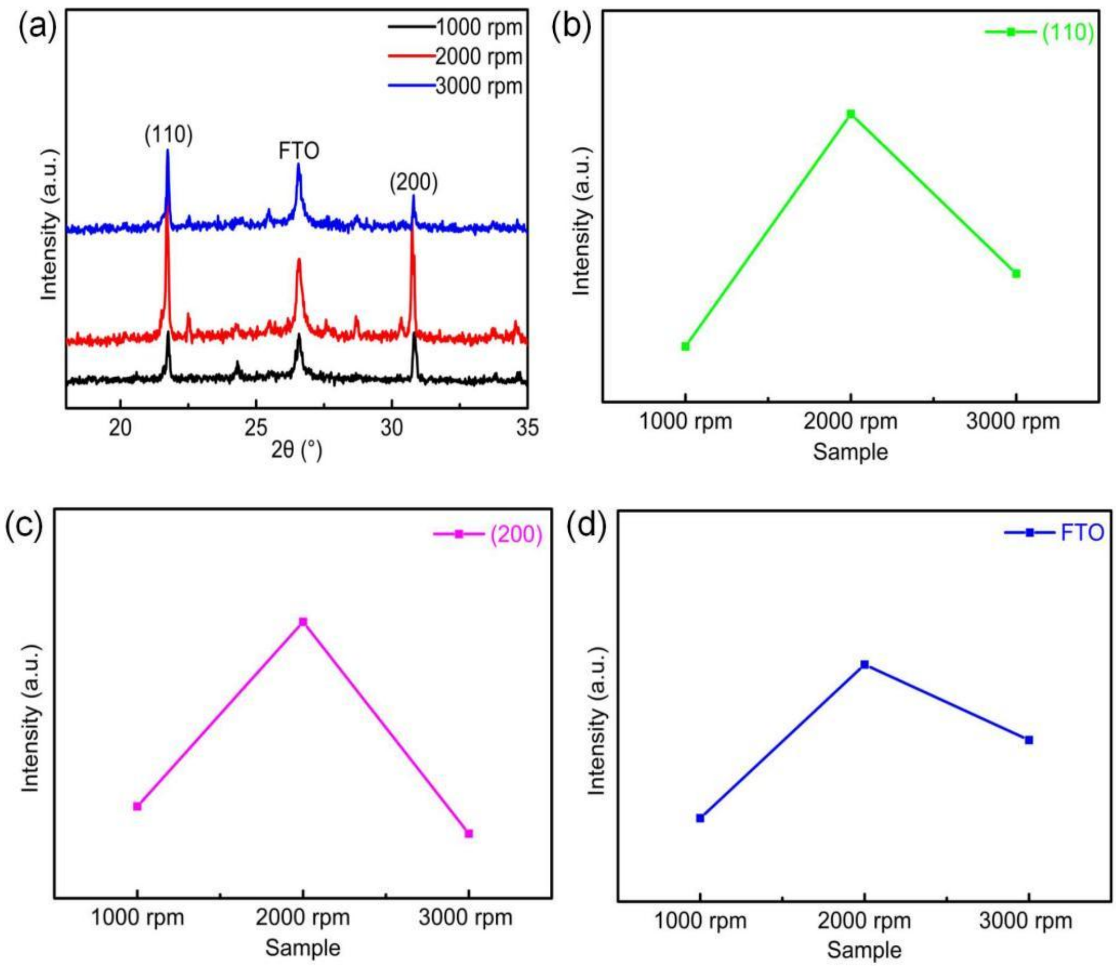

Fig. 1. (a) XRD spectra of $CsPbBr_3$ films based on different rotational speeds. Peak intensity images of (b) (110) crystallographic plane, (c) (200) crystallographic plane and (d) FTO crystallographic plane for $CsPbBr_3$ films based on different rotational speeds (colour online)

Fig. 2a-c show SEM surface images of $CsPbBr_3$ film with different rotational speeds. From Fig. 2a, it is evident that the grain distribution on the surface of the $CsPbBr_3$ film prepared at 1000rpm is inhomogeneous. In contrast, Fig. 2b demonstrates that the grain distribution on the surface of the $CsPbBr_3$ film fabricated at 2000rpm is more uniform. Nevertheless, as shown in Fig. 2c, the surface grain uniformity of the $CsPbBr_3$ film prepared at 3000rpm decreases. Table 1 shows average grain size of $CsPbBr_3$ films based on various rotational speeds. As the rotational speed increases from 1000rpm to 2000rpm, the average grain size of the $CsPbBr_3$ film improves from 405nm to 583nm. Nevertheless, when the rotational speed further increases to 3000rpm, the average grain size of the $CsPbBr_3$ film reduces to 437nm. Therefore, the $CsPbBr_3$ film prepared at a rotational speed of 3000rpm achieves optimal uniformity and the maximum average grain size. The underlying reason for the variation in the average grain size is that the reaction between the $PbBr_2$ layer and the CsBr layer is insufficient at a rotational speed of 1000rpm, resulting in the formation of a weaker $CsPbBr_3$ phase and slower grain growth. When the rotational speed increases to 2000rpm, the reaction between the $PbBr_2$ layer and the CsBr layer becomes more complete, leading to the formation of a stronger $CsPbBr_3$ phase and faster grain growth. However, as the rotational speed further increases to 3000rpm, the reaction between the $PbBr_2$ layer and the CsBr layer becomes insufficient again, resulting in a weaker $CsPbBr_3$ phase and slower grain growth.

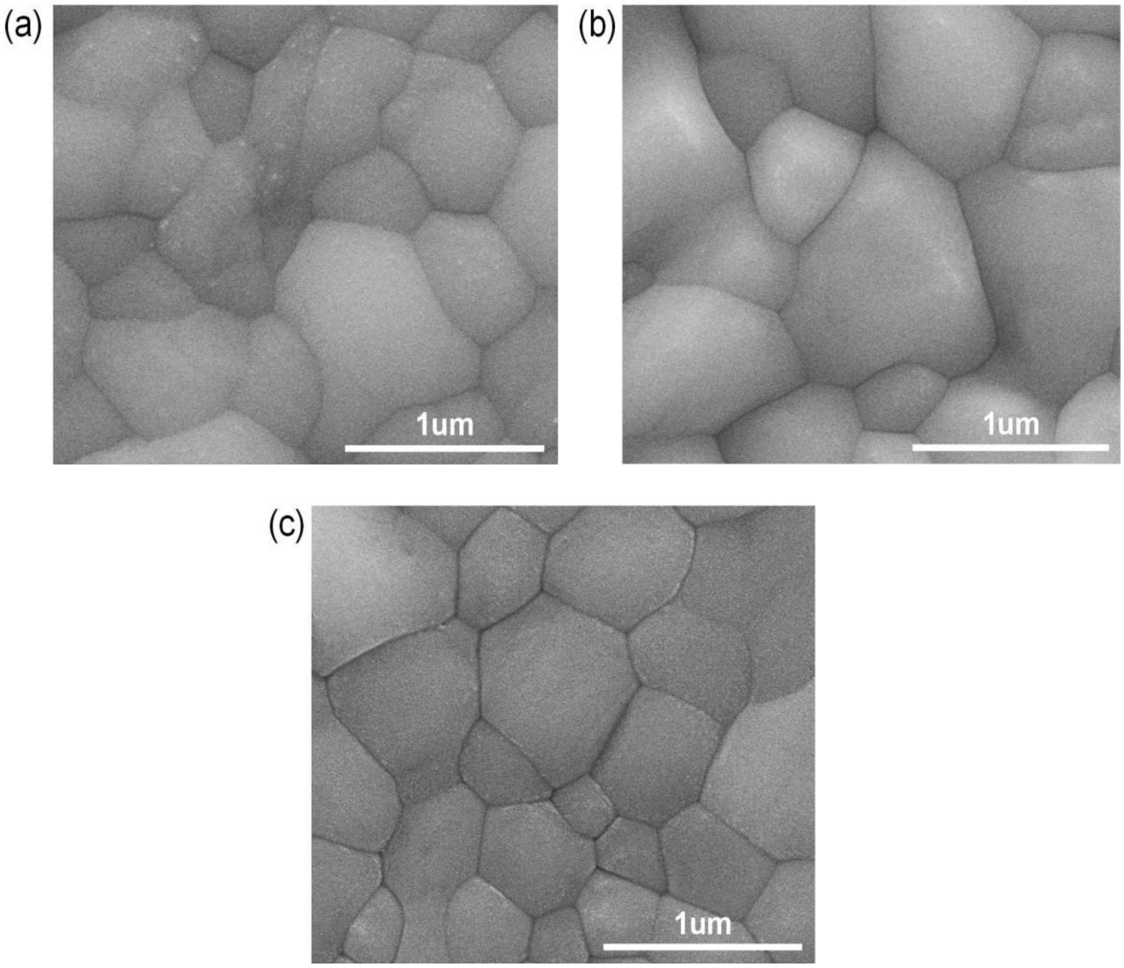

Fig. 2. SEM surface images of $CsPbBr_3$ film with (a) 1000rpm, (b) 2000rpm and (c) 3000rpm (colour online)

Table 1. Average grain sizes of $CsPbBr_3$ films based on different rotational speeds

Sample	Average grain size
1000 rpm	405 nm
2000 rpm	583 nm
3000 rpm	437 nm

Fig. 3a-c shows Cs spectra, Pb spectra and Br spectra of $CsPbBr_3$ films prepared at 2000rpm. From Fig. 3a-c, it can be seen that the $CsPbBr_3$ sample contains Cs, Pb and Br elements, indicating that there are no other impurity elements inside the prepared sample.

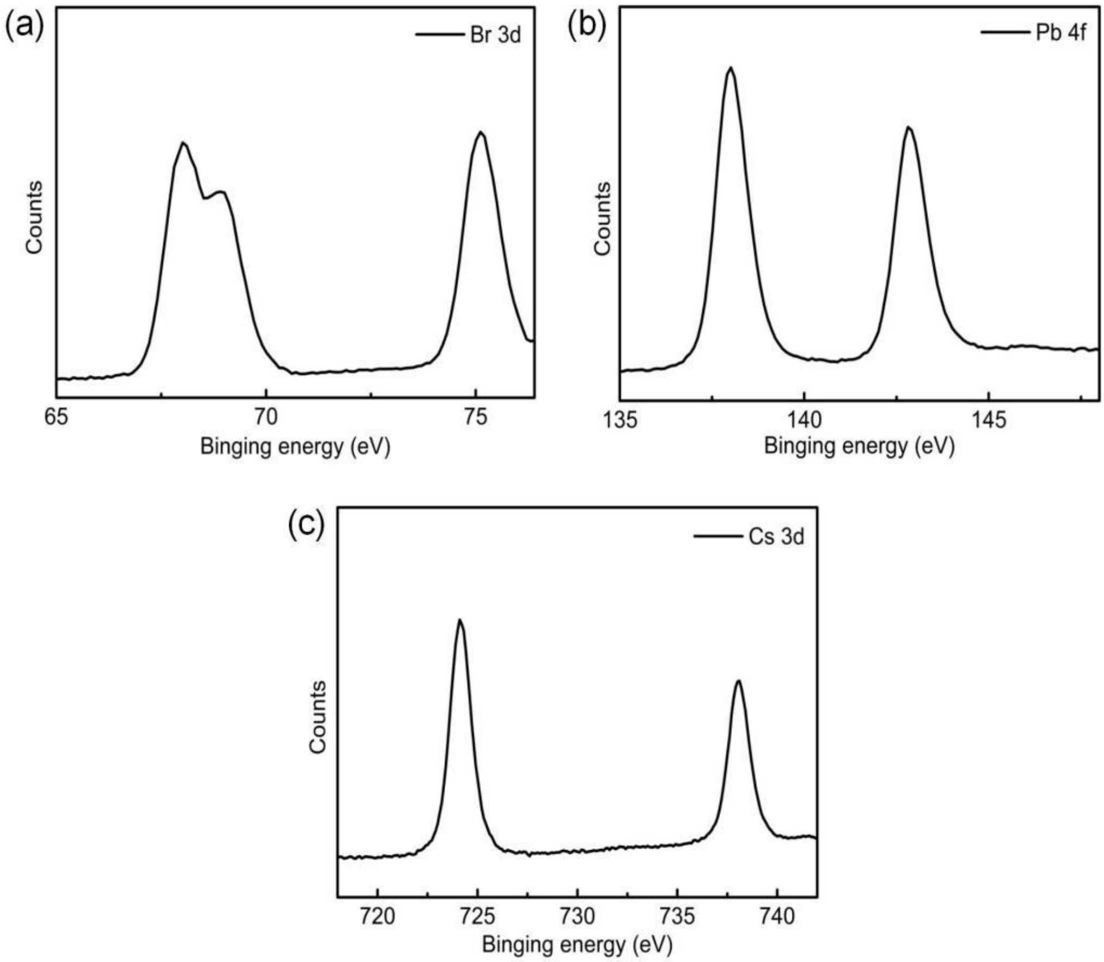

Fig. 3. (a) Br 3d spectra, (b) Pb 4f spectra and (c) Cs 3d spectra of $CsPbBr_3$ films prepared at 2000rpm

3.2. Analysis of optical properties

Fig. 4a shows absorption spectra of $CsPbBr_3$ films based on different rotational speeds. From Fig. 4a, it can be observed that the $CsPbBr_3$ film prepared at 2000rpm possesses a higher absorption rate than that of $CsPbBr_3$ film prepared at 1000rpm, implying that the $CsPbBr_3$ film fabricated at 2000rpm is capable of absorbing more solar energy. Nevertheless, the absorption rate of the $CsPbBr_3$ film prepared at 3000rpm declines, indicating a decrease in the absorbed solar energy. Thus, the $CsPbBr_3$ film prepared at 2000rpm achieves the highest absorption rate. Fig. 4b shows the relationship diagram between hv and $(ahv)^2$ for samples with different rotational speeds. The optical band gap of the $CsPbBr_3$ film was determined by further analysis of the data from Fig.4b. Fig. 4c shows optical band gaps of $CsPbBr_3$ films based on various rotational speeds. As illustrated in Fig. 4c, the $CsPbBr_3$ film prepared at 1000rpm possesses an optical band gap of 2.363eV, whereas the film fabricated at 2000rpm shows a smaller optical band gap of 2.341eV. Nevertheless, when the spin speed is too high (3000rpm), the optical band gap of the $CsPbBr_3$ film becomes larger. The decrease in the optical band gap of the $CsPbBr_3$ film indicates its capability to absorb a wider range of the light spectrum [20-26]. In contrast, the increase in the optical band gap suggests a reduction in the range of the absorption spectrum. Consequently, the $CsPbBr_3$ film prepared at 2000rpm exhibits the highest absorption rate and the smallest optical band gap.

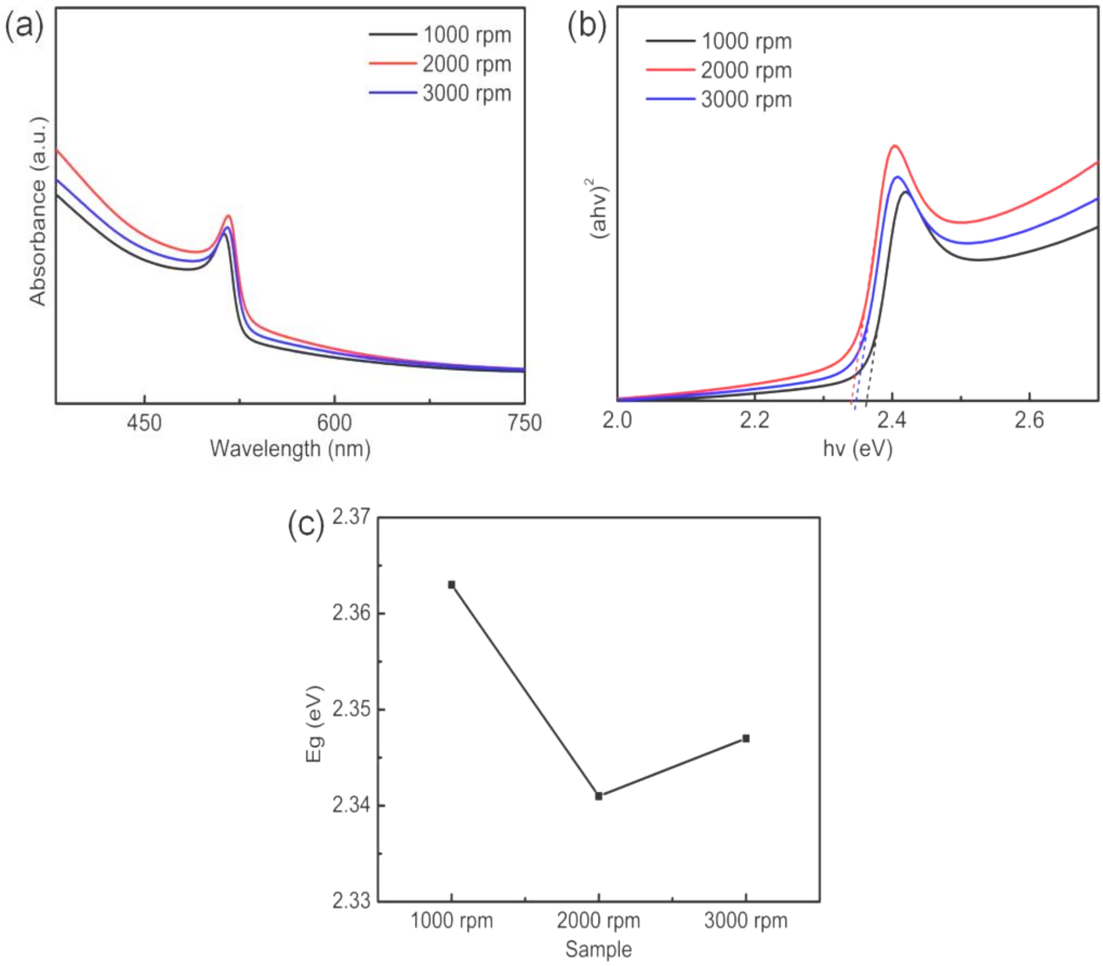

Fig. 4 (a) Absorption spectra of $CsPbBr_3$ films based on different rotational speeds. (b) The relationship diagram between hv and $(ahv)^2$ for samples with different rotational speeds. (c) Optical band gaps of $CsPbBr_3$ films based on various rotational speeds (colour online)

4. Conclusions

The high-quality $CsPbBr_3$ perovskite samples were successfully deposited via changing the rotational speed. The research results indicate that $CsPbBr_3$ sample with 2000rpm has optimum crystallinity, best uniformity, maximum average grain size (583nm) and minimum optical band gap (2.341eV) for $CsPbBr_3$ samples with 1000rpm, 2000rpm and 3000rpm. This work provides a new method for preparing high-quality $CsPbBr_3$ perovskite films.

Acknowledgements

This work was financed by the Changzhou Scientific and Technological Program grant (Grant No. CJ20250087), Project for Building a Science and Technology Innovation Center Facing South Asia and Southeast Asia (202403AP140015), the Key Applied Basic Research Program of Yunnan Province (202201AS070023) and Yunnan Revitalization Talent Support Program, the Spring City Plan: The High-level Talent Promotion and Training Project of Kunming (2022SCP005).

References

[1] C. Liu, W. Li, C. Zhang, Y. Ma, J. Fan, Y. Mai, J. Am. Chem. Soc. **140**, 3825 (2018).

[2] W. Xu, J. Hu, Q. Yang, Y. Lian, M. Zheng, E. Du, J. Alloy. Compd. **988**, 174275 (2024).

[3] F. Fei, Y. Liao, Y. Xu, S. Wang, L. Li, X. Dong, X. Zhou, J. Gao, K. Wang, N. Yuan, J. Ding, ACS Appl. Mater. Interfaces **16**, 24760 (2024).

[4] F. Zhao, Y. Guo, X. Wang, J. Tao, J. Jiang, Z. Hu, J. Chu, Sol. Energy **191**, 263 (2019).

[5] D. Wang, W. Li, Z. Du, G. Li, W. Sun, J. Wu, Z. Lan, J. Mater. Chem. C **8**, 1649 (2020).

[6] X. Chang, J. Fang, Y. Fan, T. Luo, H. Su, Y. Zhang, J. Lu, L. Tsetseris, T. Anthopoulos, S. Liu, K. Zhao, Adv. Mater. **32**, 2001243 (2020).

[7] X. Li, B. He, Z. Gong, J. Zhu, W. Zhang, H. Chen, Y. Duan, Q. Tang, Sol. RRL **4**, 2000362 (2020).

[8] A. Swarnkar, A. R. Marshall, E. M. Sanehira, B. D. Chernomordik, D. T. Moore, J. A. Christians, T. Chakrabarti, J. M. Luther, Science **354**, 92 (2016).

[9] C. Wang, A. S. Chesman, J.J. Jasieniak, Chem. Commun. **53**, 232 (2017).

[10] T. Zhang, M. I. Dar, G. Li, F. Xu, N. Guo, Y. Zhao, Sci. Adv. **3**, 1700841 (2017).

[11] Y. Guo, F. Zhao, J. Tao, J. Jiang, J. Zhang, J. Yang, Z. Hu, J. Chu, ChemSusChem **12**, 983 (2019).

[12] Y. Li, Y. Wang, T. Zhang, S. Yoriya, P. Kumnorkaew, S. Chen, X. Guo, Y. Zhao, Chem. Commun. **54**, 9809 (2018).

[13] Y. Guo, F. Zhao, X. Wang, J.Tao, D. Zheng, J. Jiang, Z. Hu, J. Chu, Sol. Energy Mater. Sol. Cell. **221**, 110918 (2021).

[14] G. Liao, J. Duan, Y. Zhao, Q. Tang, Sol. Energy **171**, 279 (2018).

[15] X. Zhang, Z. Jin, J. Zhang, D. Bai, H. Bian, K. Wang, J. Sun, Q. Wang, S.F. Liu, ACS Appl. Mater. Interfaces **10**, 7145 (2018).

[16] H. Li, G. Tong, T. Chen, H. Zhu, G. Li, Y. Chang, L. Wang, Y. Jiang, J. Mater. Chem. A **6**, 14255 (2018).

[17] J. Zhu, B. He, Z. Gong, Y. Ding, W. Zhang, X. Li, Z. Zong, H. Chen, Q. Tang, ChemSusChem **13**, 1834 (2020).

[18] Y. Xu, J. Duan, X. Yang, J. Du, Y. Wang, Y. Duan, Q. Tang, J. Mater. Chem. A **8**, 11859 (2020).

[19] F. Zhao, Y. Guo, J. Tao, Z. Li, J. Jiang, J. Chu, Appl. Optics **59**, 5481 (2020).

[20] J. Liang, C. Wang, Y. Wang, Z. Xu, Z. Lu, Y. Ma, H. Zhu, Y. Hu, C. Xiao, X. Yi, G. Zhu, H. Lv, L. Ma, T. Chen, Z. Tie, Z. Jin, J. Liu, J. Am. Chem. Soc. **138**, 15829 (2016).

[21] P. Teng, X. Han, J. Li, Y. Xu, L. Kang, Y. Wang, Y. Yang, T. Yu, ACS Appl. Mater. Interfaces **10**, 9541 (2018).

[22] X. Liu, X. Tan, Z. Liu, H. Ye, B. Sun, T. Shi, Z. Tang, G. Liao, Nano Energy **56**, 184 (2019).

[23] J. Duan, Y. Zhao, X. Yang, Y. Wang, B. He, Q. Tang, Adv. Energy Mater. **8**, 1802346 (2018).

[24] J. Gao, F. Fei, Y. Xu, S. Wang, Y. Li, K. Du, H. Sun, X. Dong, N. Yuan, L. Li, J. Ding, ACS Appl. Mater. Interfaces **16**, 38017 (2024).

[25] L. Gu, M. Chen, X. Liu, D. Chen, Y. Gu, S. Wang, Sol. RRL **8**, 2301001 (2024).

[26] L. Gu, M. Chen, X. Liu, Y. Gu, D. Chen, S. Wang, ACS Appl. Mater. Interfaces **17**, 991 (2024).

*Corresponding author: fzhaobs@126.com